01 Mar 2015

# Control of Fluid Dynamics by Nanoparticles in Laser Melting

Chao Ma

Lianyi Chen
*Missouri University of Science and Technology*, chenliany@mst.edu

Jiaquan Xu

Jingzhou Zhao

*et. al. For a complete list of authors, see https://scholarsmine.mst.edu/mec_aereng_facwork/4058*



## Recommended Citation

C. Ma et al., "Control of Fluid Dynamics by Nanoparticles in Laser Melting," *Journal of Applied Physics*, vol. 117, no. 11, American Institute of Physics (AIP), Mar 2015.
The definitive version is available at https://doi.org/10.1063/1.4915276

# Control of fluid dynamics by nanoparticles in laser melting

Chao Ma,[1] Lianyi Chen,[1] Jiaquan Xu,[2] Jingzhou Zhao,[1] and Xiaochun Li[1,2,a)]
[1]*Department of Mechanical and Aerospace Engineering, University of California at Los Angeles, Los Angeles, California 90095, USA*
[2]*Department of Materials Science and Engineering, University of California at Los Angeles, Los Angeles, California 90095, USA*

(Received 9 January 2015; accepted 6 March 2015; published online 18 March 2015)

Effective control of fluid dynamics is of remarkable scientific and practical significance. It is hypothesized that nanoparticles could offer a novel means to control fluid dynamics. In this study, laser melting was used to investigate the feasibility of tuning fluid dynamics by nanoparticles and possibly breaking existing limits of conventional laser processing techniques. Alumina nanoparticles reinforced nickel samples, fabricated through electrocodeposition, were used for laser melting experiments. Since the melt pool surface is controlled by the fluid dynamics, surface topographies were carefully studied to reveal the nanoparticle effect on the fluid dynamics. Characterizations of surface topographies and microstructures of pure Ni and Ni/$Al_2O_3$ nanocomposite were carried out before and after laser melting. The surface roughness of the Ni/$Al_2O_3$ nanocomposite sample was reduced significantly by laser melting, which broke the existing limit of laser surface polishing of pure Ni. It is believed that the nanoparticles increased the viscosity of the molten metal, thereby enhancing the viscous damping of the capillary oscillations in the melt pool, to produce a much smoother surface. Moreover, the experimental study also revealed that the viscosity enhancement by the nanoparticles effectively suppressed the thermocapillary flows which would introduce artificial asperities on a surface. The experimental results suggest that nanoparticles are effective in controlling melt pool dynamics and overcoming the existing limits of laser processing. The new methodology, fluid dynamics control by nanoparticles, opens a new pathway to enrich liquid based processes for broad applications.
 [http://dx.doi.org/10.1063/1.4915276]

## I. INTRODUCTION

Fluid dynamics is of remarkable scientific and practical significance given that the vast majority of the observable mass in the universe exists in a fluid state. Fluid dynamics plays a crucial role in numerous applications including transportation, power generation and conversion, material processing and manufacturing, food production, pharmacy, and civil infrastructure.[1] Effective control of fluid dynamics is thus of significant value. Recent studies have shown that thermophysical properties of a bulk material can be tailored by the additions of nanoparticles.[2–8] It is thus believed that nanoparticles could offer a novel means to control fluid dynamics.

Laser melting is used in this study to investigate the feasibility to control fluid dynamics using nanoparticles. Laser can be readily used to create a dynamic melt pool, which has tremendous applications already.[9–13] This study is also motivated by an intriguing hypothesis that the introduction of nanoparticles in the laser-induced melt pool would break fundamental limits in some laser processing technologies through effective control of the melt pool flow. For example, fundamental barriers exist in some laser melting processes, such as laser polishing and laser patterning of metals, which limit the surface conditions that can be possibly achieved (e.g., residual roughness,[12,13] gloss,[14] and reflectivity[15]). Latest studies have shown that these barriers are related to melt pool dynamics such as damped capillary oscillations[16,17] and thermocapillary (Marangoni) flows[18–21] in melt pools, which are significantly influenced by thermophysical properties (e.g., viscosity and surface tension) of the metal melt. Therefore, there is an opportunity to break the limits/barriers of current laser material processing technologies by tuning melt pool dynamic behavior using nanoparticles, possibly significantly broadening laser melting capability and application space.

As one of the laser melting applications, laser polishing has been extensively studied as a non-contact surface smoothing technology.[13–28] Laser polishing is advantageous over traditional polishing techniques in many aspects: high speed, great reproducibility, and fully automatic control. In addition, it is able to polish curved and even concave surfaces while leave no residues. A large number of existing studies[14,15,24–28] on laser polishing aimed to determine the parameters that result in the best surface finish. The studies suggest there exists a fundamental limit on the reduction of roughness achievable by laser polishing. The resultant surface topography by laser polishing is dictated by the dynamics of melt pool flow,[16–21] which is governed by laser parameters and the thermophysical properties of the material. The surface quality achievable by laser polishing is limited merely by optimization of laser parameters. Nanoparticles could be added into the base material to modify the thermophysical properties to control the laser-induced melt pool

a)Author to whom correspondence should be addressed. Electronic mail: xcli@seas.ucla.edu.

 

dynamics, providing a new pathway to break existing limit for surface smoothing.

The methodology, control of fluid dynamics by nanoparticles, will be valuable not only in laser material processing (e.g., laser welding, selective laser melting, laser texturing, laser cladding, etc.) but also for any applications where fluid dynamics is involved, such as electron beam material processing and arc welding. For example, in welding, the surface tension coefficient of the base metal or alloy determines the direction of thermocapillary flows and thus significantly affects the weld penetration.[29] It is believed that nanoparticles can be engineered to tune the surface tension coefficient and thus to increase the penetration depth. This research will also contribute to the knowledge of how laser interacts with metal matrix nanocomposites (MMNCs), which is emerging as an important class of metallic materials with significantly enhanced mechanical, thermophysical, and electrical properties.

## II. THEORETICAL BACKGROUND

Previous studies suggest that there exist two kinds of fluid flow patterns in a laser-induced melt pool: damped capillary oscillations and thermocapillary flows, as schematically shown in Fig. 1. The melt pool flow is dominated by capillary oscillations (Fig. 1(a)) at low laser energies where is defined as Capillary Regime.[16,17] In the capillary regime, a surface is smoothed through damping of capillary oscillations based on viscous dissipation. The amplitude $\zeta$ of the oscillatory wave decays exponentially with time $t$

$$\zeta(t) = \zeta(0)e^{-\gamma t}. \tag{1}$$

The damping coefficient $\gamma$ is given as

$$\gamma = \frac{2\mu\kappa^2}{\rho}, \tag{2}$$

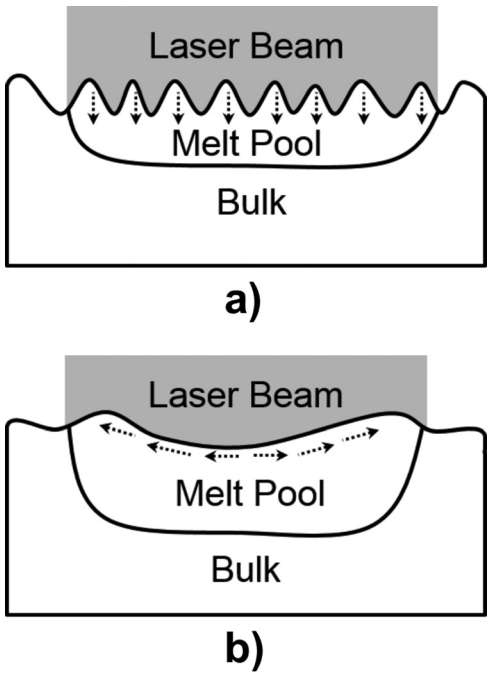


FIG. 1. Schematics of melt pool flows: (a) damped capillary oscillation and (b) thermocapillary flow.

where $\mu$ and $\rho$ are the dynamic viscosity and the density of the molten metal, respectively, and $\kappa$ is the wave number of the oscillation that is dependent on the wavelength $\lambda$, $\kappa = 2\pi/\lambda$. In the capillary regime, the surface roughness decreases with increasing energy because the surface capillary waves are damped more significantly due to the increased melting time.

However, as the energy increases to a certain level, thermocapillary flows (Fig. 1(b)) begin to dominate the melt pool flow, where is defined as Thermocapillary Regime.[18–21] Thermocapillary flows occur only if the surface tension gradient overcomes the viscous force

$$-\frac{d\sigma}{dT}\frac{\partial T}{\partial r} = \mu\frac{\partial v_s}{\partial z}, \tag{3}$$

where $\sigma$ is the surface tension, $T$ is the temperature, $r$ and $z$ are the positions in cylindrical coordinates, $\mu$ is the dynamic viscosity, and $v_s$ is the surface velocity in the radial direction. In the thermocapillary regime, the molten metal flows along the radial direction of the melt pool due to the surface tension gradient induced by a large temperature gradient. The surface asperities can be smoothed by the radial thermocapillary flows. However, the thermocapillary flows also introduce ripples and thereby increase surface roughness. This is why the surface roughness eventually increases with increasing laser energy.

## III. EXPERIMENTAL METHODS

### A. Preparation of metal matrix nanocomposite samples

Ni/$Al_2O_3$ nanocomposite was prepared by electrocodeposition[30] of Ni and $Al_2O_3$ nanoparticles in a standard nickel Watts bath containing 10 g/l of spherical $Al_2O_3$ nanoparticles with an average diameter of about 50 nm. The solution containing $Al_2O_3$ nanoparticles was mechanically mixed and ultrasonically processed for 2 h prior to electrocodeposition to achieve a uniform distribution and effective dispersion of the nanoparticles. Electrocodeposition was carried out for 2 h with the continuation of mechanical stirring and sonication to maintain the nanoparticle dispersion and distribution. The temperature was controlled at 43 °C and the current density was set at 1 A/$dm^2$. Pure Ni was also prepared under the same conditions for a comparative study.

### B. Pulsed laser micro melting

A 1070-nm, 200 -W fiber laser (SPI Lasers SP-200 C-A-S6-A-C) was used for pulsed laser micro melting experiments. The laser was directed into a scan head (ScanLab HurryScan III 14 mm) to allow for high-speed scan at a beam velocity of up to 2 m/s. The scan head was controlled by a PCI control card and furnished with an f-theta objective with a focal length of 163 mm. The laser was pulsed at a frequency of 100 kHz and a pulse duration of 1.5 $\mu$s. The laser beam diameter was about 48.8 $\mu$m at the working plane. A raster scan was carried out with a track offset of 4 $\mu$m and a scan speed of 0.4 m/s. Ultrahigh-purity argon was flown over the samples during laser melting to minimize chemical

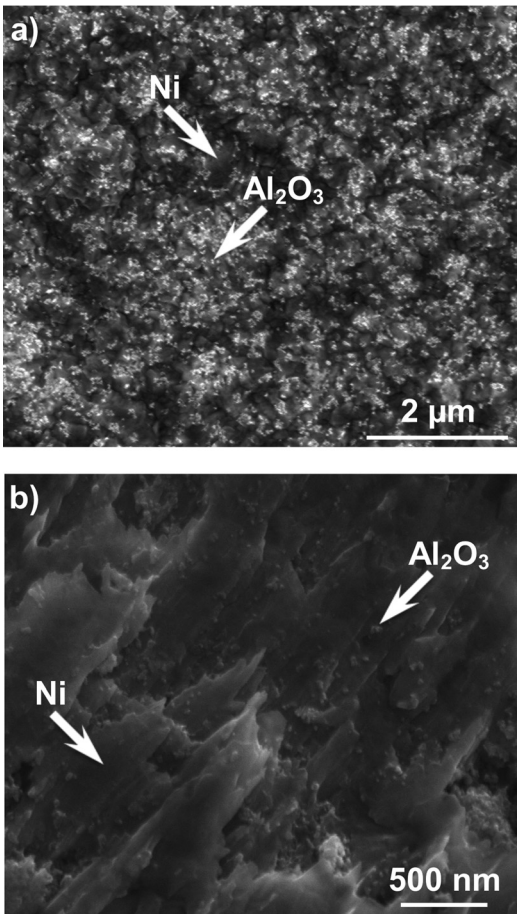


FIG. 2. SEM micrographs of electrocodeposited $Ni/Al_2O_3$ nanocomposite (a) surface and (b) cross section.

reactions between the samples and air. Both pure Ni and $Ni/Al_2O_3$ nanocomposite samples were laser melted to investigate the effects of $Al_2O_3$ nanoparticles on the dynamics of the melt pool. Laser melting experiments were conducted at different energies while other parameters were maintained constant.

### C. Characterization

The surface topographies of pure Ni and $Ni/Al_2O_3$ nanocomposite before and after laser melting were measured with white light interferometry. The metric for evaluating the surface finish was the arithmetic average roughness (Sa) based on an areal measurement of surface height, which was calculated by following the ASME standard. Areal surface roughness (e.g., Sa) is preferable to linear surface roughness (e.g., Ra), because it characterizes the surface conditions over an entire area. Five measurements were made at different locations for each specimen and an average value was taken to diminish the location variation effect. Characterization of micro/nano-structures of the samples was carried out using scanning electron microscopy (SEM) facilitated with energy dispersive X-ray spectroscopy (EDS/EDX). EDS analysis was used to quantify the fraction of $Al_2O_3$ nanoparticles incorporated into Ni matrix. The cross section of the laser processed region was cut by focused ion beam (FIB) and characterized with SEM.

## IV. RESULTS AND DISCUSSION

### A. Microstructure of $Ni/Al_2O_3$ nanocomposite before laser melting

The SEM micrographs of the $Ni/Al_2O_3$ nanocomposite before laser melting are shown in Fig. 2. The $Al_2O_3$ nanoparticles (the discontinuous bright phases) are evenly distributed in the Ni matrix (the dark continuous phases) without large clusters, indicating an effective dispersion of nanoparticles. By characterization of the fractured cross section of the $Ni/Al_2O_3$ coating, it shows $Al_2O_3$ nanoparticles are present all over the entire sample, which suggests a uniform incorporation process. An excellent dispersion and distribution of nanoparticles are necessary to achieve remarkable laser melting results because nanoparticle clusters are not as effective as dispersed nanoparticles in modification of thermophysical properties of the base metal and nanoparticle clusters themselves could introduce significant surface asperities. With the atom fractions Al and Ni in the nanocomposite measured by EDS, the volume fraction of $Al_2O_3$ nanoparticles was estimated to be $4.4\% \pm 0.1\%$.

### B. Surface topography

Laser melting experiments were carried out on Ni and $Ni/Al_2O_3$ with various pulse energies. The effects of nanoparticles on melt pool flow can be directly revealed by observation of the specific surface topographies of Ni and $Ni/Al_2O_3$. Fig. 3 shows the representative surface topographies of Ni and $Ni/Al_2O_3$ before laser melting, with the surface height data (Z) represented by different colors in reference to the X-direction and Y-direction. The $Ni/Al_2O_3$ nanocomposite is rougher than the pure Ni although they were deposited under the same condition. The average surface roughness of Ni over five locations is 254 nm and that of $Ni/Al_2O_3$ is 323 nm. The difference is probably because the addition and

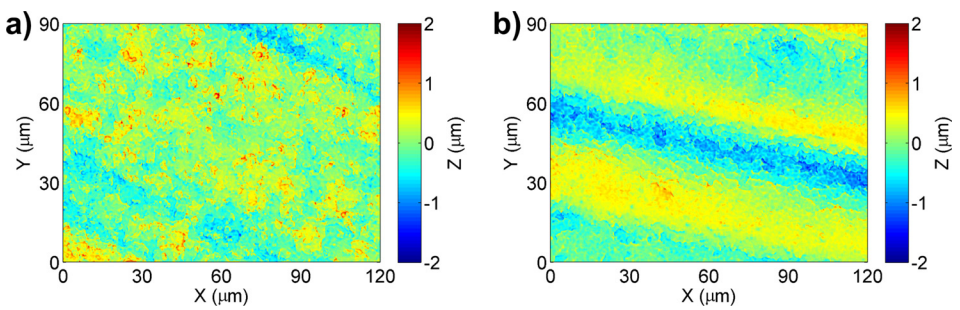


FIG. 3. Surface topographies of (a) Ni and (b) $Ni/Al_2O_3$ before laser melting.

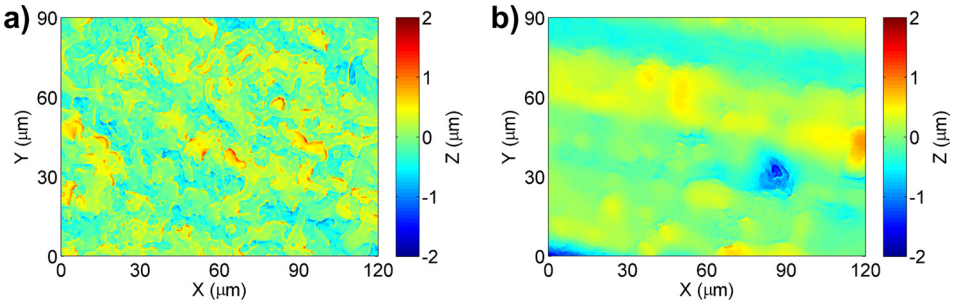


FIG. 4. Surface topographies of (a) Ni and (b) $Ni/Al_2O_3$ after laser melting at 0.10 mJ per pulse.

incorporation of $Al_2O_3$ nanoparticles distort the electrical field for electrodeposition.

Fig. 4 shows the typical surface topographies of Ni and $Ni/Al_2O_3$ that were laser melted at the lowest pulse energy used in this study (0.10 mJ). The $Ni/Al_2O_3$ nanocomposite was more significantly melted than the pure Ni. It is possible that the $Ni/Al_2O_3$ nanocomposite absorbed the laser energy more efficiently due to its higher surface roughness than pure Ni. Additionally, the presence of $Al_2O_3$ nanoparticles could have decreased the effective thermal conductivity of the nanocomposites by scattering of electrons and phonons that conduct heat. The decreased thermal conductivity would prevent efficient heat transfer to bulk and thus help with heat accumulation within the surface. In addition, the presence of nanoparticles increased the viscosity of the molten metal, which also resulted in more damping of capillary waves and thus more reduction of surface asperities.

Fig. 5 shows the surface topographies of Ni and $Ni/Al_2O_3$ that were laser melted at a higher energy (0.14 mJ). Compared with those in Fig. 4, the surface asperities were more significantly reduced because increased energy results in increased melt duration for damping of the surface waves. Again, after melted under the same conditions, $Ni/Al_2O_3$ has smaller average surface roughness than Ni. The greater reduction of roughness in $Ni/Al_2O_3$ should be due to the increased viscosity by the nanoparticles and thereby an enhanced damping of capillary waves. Although the laser melted surfaces in Fig. 5 were much smoother than the original surfaces in Fig. 3, there still remained some low-frequency asperities, which could be reduced by a higher laser energy.

The surface topographies of Ni and $Ni/Al_2O_3$ melted at an even higher energy (0.18 mJ) are shown in Fig. 6. The increased energies induced more significant melting such that the low-frequency asperities are considerably reduced compared with Fig. 5. However, the mechanisms for reducing the asperities in Ni and $Ni/Al_2O_3$ are different: the thermocapillary regime for Ni and the capillary regime for $Ni/Al_2O_3$. Noticeably, by comparison between Figs. 6(a) and 6(b), laser melting introduced more significant ripples in pure Ni than $Ni/Al_2O_3$. The ripples resulted from thermocapillary flows in the melt pool. In order for thermocapillary flows to occur, the surface tension gradient along the radial direction of the melt pool has to overcome the viscous force of the molten metal. Since $Al_2O_3$ nanoparticles can increase the viscosity, it is more difficult to form thermocapillary flows in the melt pool of $Ni/Al_2O_3$ than that of Ni. In addition, it has been extensively reported that the presence of oxygen content reduces the surface tension of liquid metals.[31–33] It is possible that the $Al_2O_3$ nanoparticles reduced the surface tension and thus the surface tension coefficient of Ni melt, which further suppressed thermocapillary flow. Therefore, addition of $Al_2O_3$ nanoparticles delayed the onset of thermocapillary flows and enlarged the processing window of the capillary regime. This is of great significances and benefits in laser polishing because a surface is smoothed at no cost in the capillary regime while at the cost of introducing artificial ripples/asperities in the thermocapillary regime. This is why the resultant surface roughness of $Ni/Al_2O_3$ is much smaller than that of Ni. This pulse energy (0.18 mJ) was the optimal parameter for $Ni/Al_2O_3$.

As the energy per laser pulse was further increased, the surface roughness of Ni decreased while that of $Ni/Al_2O_3$ increased, which is shown in Fig. 7. By comparison between Figs. 6(a) and 7(a), the Ni surface was smoothed by increasing laser energy because the low-frequency asperities were reduced more significantly by stronger thermocapillary flows. This pulse energy (0.22 mJ) was the optimal parameter for Ni, and a further increase in the pulse energy would induce a rougher surface because excessive ripples were introduced by thermocapillary flow. In the case of $Ni/Al_2O_3$, as the pulse energy was increased from 0.18 mJ (Fig. 6(b)) to 0.22 mJ (Fig. 7(b)), it triggered the onset of thermocapillary flow. The thermocapillary flows at 0.22 mJ played a role in

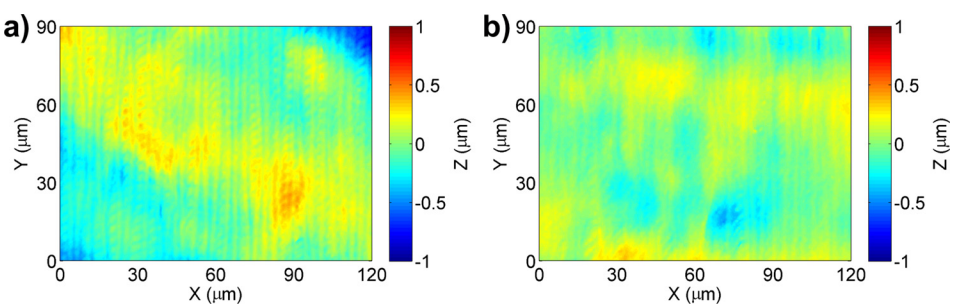


FIG. 5. Surface topographies of (a) Ni and (b) $Ni/Al_2O_3$ after laser melting at 0.14 mJ per pulse.

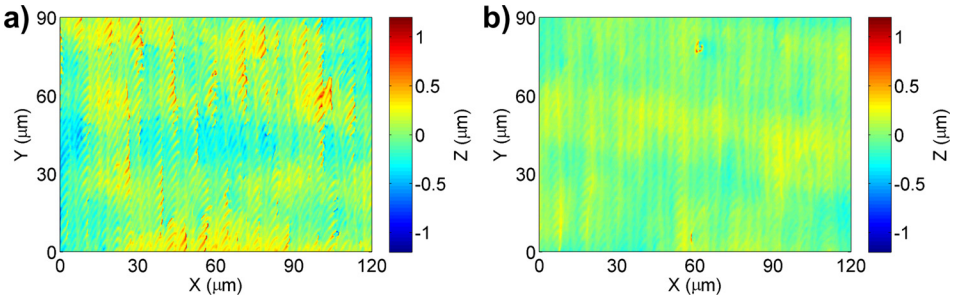


FIG. 6. Surface topographies of (a) Ni and (b) Ni/$Al_2O_3$ after laser melting at 0.18 mJ per pulse.

roughening instead of smoothing since the Ni/$Al_2O_3$ surface was already fairly smooth at 0.18 mJ.

### C. Surface roughness

Surface roughnesses were calculated based on the surface topographies acquired with white light interferometry. Fig. 8 shows the normalized surface roughness of Ni and Ni/$Al_2O_3$ versus laser energy per pulse. It should be noted that the normalized roughnesses were the absolute roughnesses divided by the roughness of the corresponding original surface before laser melting. A normalized roughness value of less than 1 indicates that the laser melted surface is smoother than the original surface, i.e., polishing.

The surface roughnesses of Ni and Ni/$Al_2O_3$ follow the same trend with increasing pulse energy: the surface roughnesses decrease at low energies and then increase at high energies. The minimum values mean the best polishing results. The minimum normalized roughnesses achieved on Ni and Ni/$Al_2O_3$ are 0.42 and 0.22, respectively. The addition of $Al_2O_3$ nanoparticles in laser melting process reduced the normalized roughness nearly by a factor of 2, or rather, the polishability was doubled by tuning the fluid dynamics of the melt pool by nanoparticles. In terms of the absolute values, the surface roughness of Ni was reduced from 254 nm to 107 nm with the optimal parameters while that of Ni/$Al_2O_3$ was reduced from 323 nm to 72 nm. The key results on laser melting of Ni and Ni/$Al_2O_3$ are listed in Table I.

Figs. 9 and 10 show the spatial frequency spectra of the Ni and Ni/$Al_2O_3$ surfaces that are laser melted at various energies. The spatial frequency spectra are cross sections of two-dimensional fast Fourier transforms (FFTs) of the surface height data from the topography measurements. The X-direction and Y-direction are perpendicular and parallel to the raster scan lines, respectively. The spectra at different energies are presented with an even offset between each other to allow for clarity. For the original surfaces of Ni and Ni/$Al_2O_3$, the surface roughnesses are mostly contributed by the asperities from the Y-direction spectra (Figs. 9(b) and 10(b)). As the laser energy increases, the original asperities are reduced in the Y-direction spectra, but artificial features are also added in the X-direction spectra (Figs. 9(a) and 10(a)), especially for the high laser energies (e.g., 0.22 mJ). There exist optimal parameters for the balance of both effects, which are corresponding to the minima in Fig. 8. The resultant surface topographies by laser melting are dictated by the melt pool flow, which is discussed as follows, with a focus on the difference between Ni and Ni/$Al_2O_3$.

Viscosity plays a crucial role in both the capillary and thermocapillary regimes as reviewed in Sec. II. Since the introduction of nanoparticles increases the viscosity of a liquid[5], the melt pool dynamics can be controlled by nanoparticles. In this work, the addition of nanoparticles increased the magnitude of viscous damping in the capillary regime and thus resulted in a smoother surface for Ni/$Al_2O_3$ than Ni as shown in Fig. 8. In addition, the nanoparticles suppressed thermocapillary flows by increasing viscosity and thus enlarged the processing window of the capillary regime, which is clearly illustrated by analysis of the spatial frequency spectra in Figs. 9 and 10.

The transition energies between the capillary and thermocapillary regimes of Ni and Ni/$Al_2O_3$ can be determined by examining the asperities introduced by thermocapillary flows. If thermocapillary flows were developed, a peak would be introduced to the spatial frequency spectra at the frequency associated with the scan line spacing. The offset between scan lines in the laser melting experiments was 4 $\mu$m, which is corresponding to a spatial frequency of 250 $mm^{-1}$ perpendicular to the scan tracks and marked as black dashed lines in Figs. 9(a) and 10(a). The peaks at this certain spatial frequency can be considered as signatures of thermocapillary flows. The frequencies can be slightly off due to positioning error of the scan head and measurement error of the white light interferometer. In the case of Ni in Fig. 9(a), the peak is not evident at 0.10 mJ, and initiated at

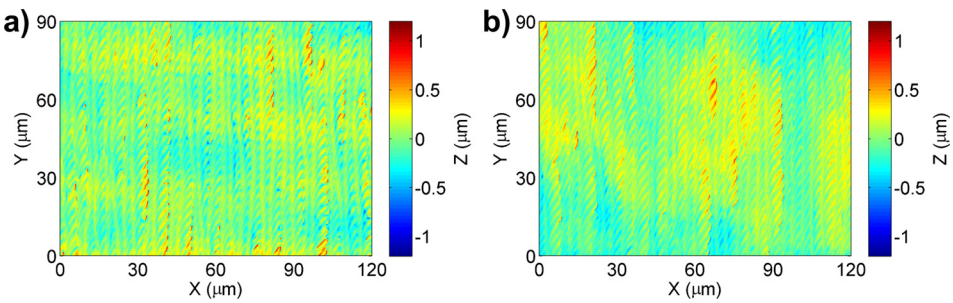


FIG. 7. Surface topographies of (a) Ni and (b) Ni/$Al_2O_3$ after laser melting at 0.22 mJ per pulse.

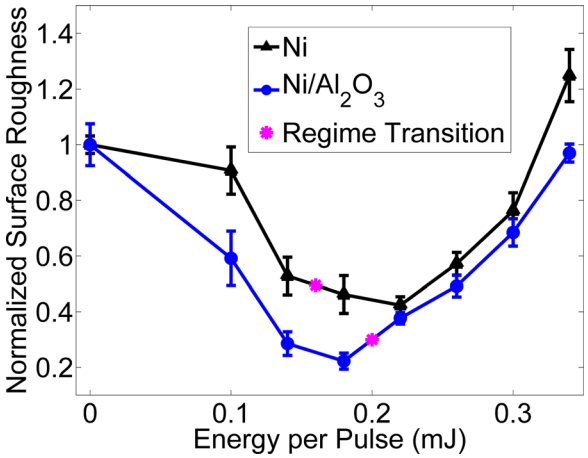


FIG. 8. Normalized surface roughness of pure Ni and $Ni/Al_2O_3$ v.s. pulse energy.

0.14 mJ and fully developed at 0.18 and 0.22 mJ. For $Ni/Al_2O_3$ in Fig. 10(a), the peak is initiated at 0.18 mJ and fully developed at 0.22 mJ. Therefore, the transition energy between two regimes was defined as 0.14–0.18 mJ in Ni while 0.18–0.22 mJ in $Ni/Al_2O_3$. The thermocapillary flows were suppressed by nanoparticles and therefore the processing window of the capillary regime was extended.

As a result of the viscosity enhancement effect of nanoparticles, the best polishing on $Ni/Al_2O_3$ was achieved in the capillary regime, which smoothed the asperities of almost all frequencies and reduced the surface roughness significantly. In the case of Ni, the capillary regime was less effective and merely smoothed the asperities at high frequency. Thermocapillary flows must be used to reduce the low-frequency features and artificial asperities were introduced, thereby resulting in a higher surface roughness than $Ni/Al_2O_3$. The significant improvement in surface finish by the introduction of $Al_2O_3$ nanoparticles proved the possibility to control fluid dynamics by nanoparticles and thus break the existing limits of laser material processing.

### D. Microstructure of $Ni/Al_2O_3$ nanocomposite after laser melting

To characterize the cross section of the laser melted $Ni/Al_2O_3$ nanocomposite sample, the laser melted region was cut open by focused ion beam (FIB). The SEM micrograph of the $Ni/Al_2O_3$ specimen laser melted at 0.18 mJ is shown in Fig. 11. There exists a clear boundary between the melted and unmelted regions, which is marked as a white dashed line. There are less nanoparticles in the laser melted zone than the unmelted zone, which agrees well with the

TABLE I. Key results on laser melting of Ni and $Ni/Al_2O_3$.

| Material | Original roughness (nm) | Pulse energy (mJ) | Melting regime | Achievable roughness (nm) | Normalized roughness |
|---|---|---|---|---|---|
| Ni | 254 | 0.22 | Thermocapillary | 107 | 0.42 |
| $Ni/Al_2O_3$ | 323 | 0.18 | Capillary | 72 | 0.22 |

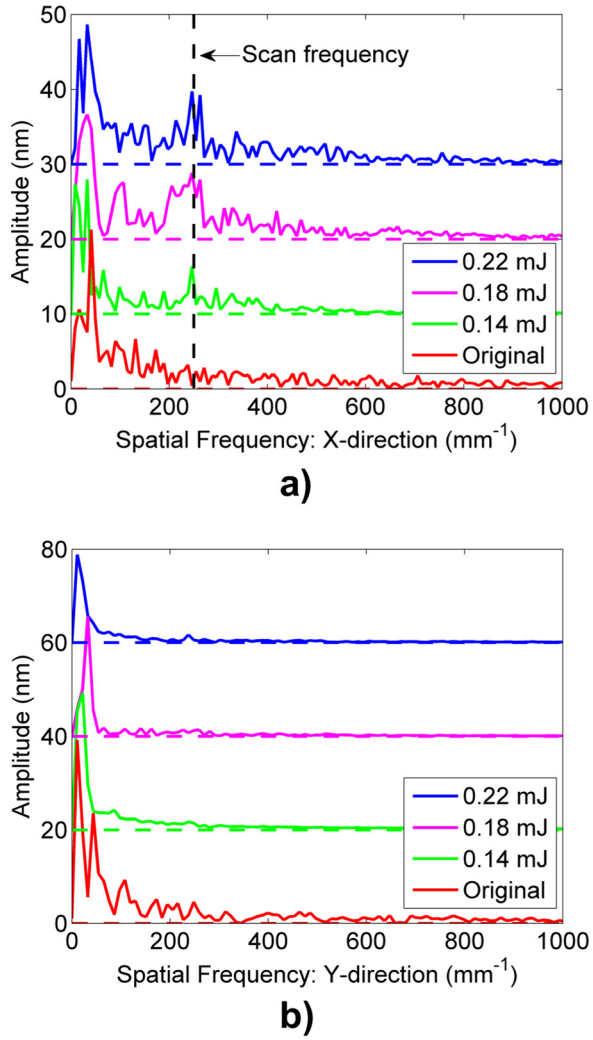


FIG. 9. Spatial frequency spectra of Ni surface before and after laser melting at various pulse energies: (a) X-direction and (b) Y-direction.

characterization results on the surface of the sample in Fig. 12. Based on the difference in microstructure, the laser melt depth is estimated to be 2.1 $\mu$m. It shows pulsed laser micro melting only smooths the surface and leaves the bulk material unaffected.

Fig. 12 shows SEM micrographs of the surface of the laser melted $Ni/Al_2O_3$ nanocomposite at 0.18 mJ. The dark particles are the $Al_2O_3$ phases. Compared with the original $Ni/Al_2O_3$ nanocomposite in Fig. 2, the quantity of $Al_2O_3$ decreased considerably after laser melting. The EDS analysis showed that the ratio of Al to Ni decreased by ~2/3. In the raster scan process, the laser scan speed and the track offset were set to obtain ~80% overlap in both directions (i.e., parallel and perpendicular to the scan tracks). Because of such a large overlap in both directions, the sample was actually melted and solidified multiple times (~5 times in each direction, i.e., ~10 times in total). Due to repetitive melting and solidification, the $Al_2O_3$ nanoparticles could have decomposed into Al and O and dissolved in the molten Ni. The dissolved Al probably partially evaporated, and the remaining Al re-precipitated as $Al_2O_3$. It is also possible that some $Al_2O_3$ nanoparticles agglomerated and ejected from the melt pool. The exact mechanism for the vanishing of $Al_2O_3$

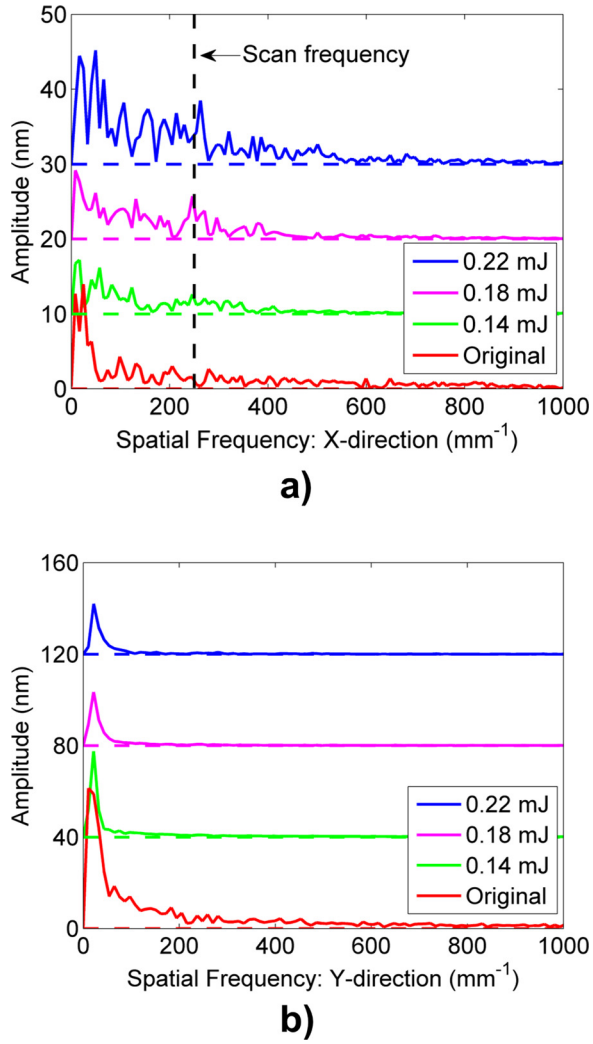


FIG. 10. Spatial frequency spectra of Ni/$Al_2O_3$ surface before and after laser melting at various pulse energies: (a) X-direction and (b) Y-direction.

nanoparticles is under further investigation. Although partial $Al_2O_3$ nanoparticles disappeared, the remaining nanoparticles still played an important role in the enhancement of the viscosity of the melt.

The $Al_2O_3$ nanoparticles are selected in this work because the electrocodeposition parameters are well established with which the nanoparticles can be successfully incorporated and effectively dispersed. The high quality of

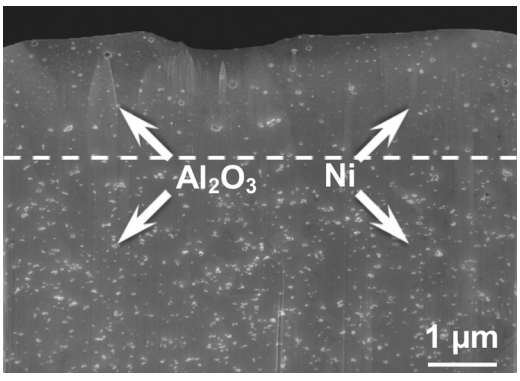


FIG. 11. SEM micrographs of the surface of the laser melted Ni/$Al_2O_3$ nanocomposite at 0.18 mJ.

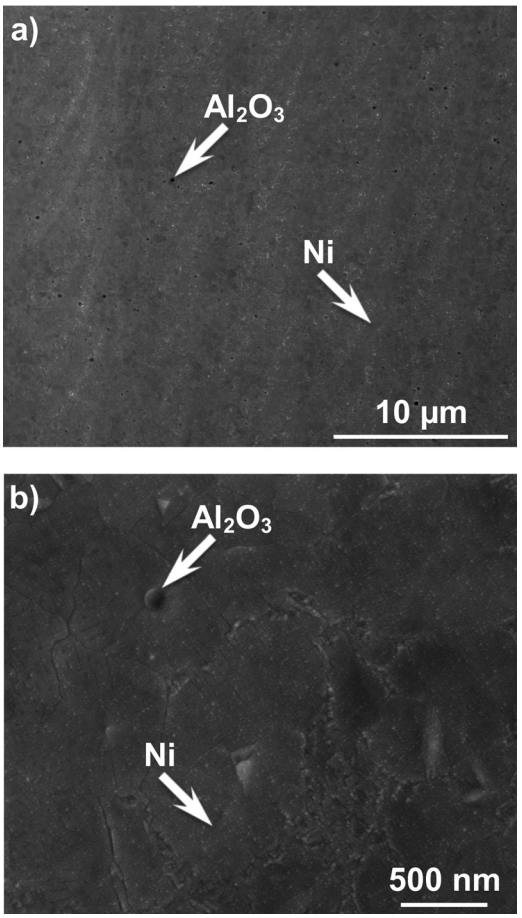


FIG. 12. SEM micrographs of the cross section of the laser melted Ni/$Al_2O_3$ nanocomposite at 0.18 mJ at (a) low and (b) high magnifications.

the nanocomposite sample is crucial for the nanoparticles to have a significant effect on the thermophysical properties of the base metal. Viscosity is the most important property tuned by nanoparticles in the present work. According to Corcione's empirical equation based experimental data of nanofluids,[5] the viscosity of a composite only depends on the size and the volume fraction of the nanoparticles, not much on the material of the nanoparticles. The effective viscosity of a nanofluid increases as the size of nanoparticles decreases and the fraction of nanoparticles increases. However, the laws of nanoparticle-modified viscosity in metal melts remain to be understood, including the effects of the material, size, and fraction of nanoparticles, which will be studied in future.

## V. CONCLUSIONS

Controlling fluid dynamics by nanoparticles was successfully demonstrated in laser surface melting of metal matrix nanocomposites, which was fabricated through electrocodeposition. The fundamental limit in laser surface smoothing, i.e., polishing, was overcome by tuning the fluid dynamics of the melt pool via nanoparticles. With nanoparticles, the onset of thermocapillary flows in laser melting was delayed and thus the processing window of the capillary regime was enlarged. In addition, the smoothing efficiency in the capillary regime was enhanced due to the addition of

nanoparticles. With help of nanoparticles, the capillary regime was effective to smooth out the asperities of $Ni/Al_2O_3$ nanocomposite, resulting in a normalized surface roughness of 0.22, which was much smaller than the minimum value achieved in pure Ni, i.e., 0.42. Therefore, by introduction of nanoparticles and modification of thermophysical properties, it opens a new pathway to extend the capability and broaden the application space of liquid based processes. The methodology, control of fluid dynamics by nanoparticles, will be valuable in many fields wherever fluid dynamics plays a crucial role.


[1]P. K. Kundu, I. M. Cohen, and D. R. Dowling, *Fluid Mechanics* (Academic, Waltham, 2012).
[2]S. Vafaei, A. Purkayastha, A. Jain, G. Ramanath, and T. Borca-Tasciuc, Nanotechnology **20**, 185702 (2009).
[3]S. Vafaei, T. Borca-Tasciuc, M. Z. Podowski, A. Purkayastha, G. Ramanath, and P. M. Ajayan, Nanotechnology **17**, 2523 (2006).
[4]S. J. Kim, I. C. Bang, J. Buongiorno, and L. W. Hu, Appl. Phys. Lett. **89**, 153107 (2006).
[5]M. Corcione, Energ. Convers. Manage. **52**, 789 (2011).
[6]B. Poudel, Q. Hao, Y. Ma, Y. Lan, A. Minnich, B. Yu, X. Yan, D. Wang, A. Muto, D. Vashaee, X. Chen, J. Liu, M. S. Dresselhaus, G. Chen, and Z. Ren, Science **320**, 634 (2008).
[7]K. Biswas, J. He, I. D. Blum, C. I. Wu, T. P. Hogan, D. N. Seidman, V. P. Dravid, and M. G. Kanatzidis, Nature **489**, 414 (2012).
[8]M. Zebarjadi, G. Joshi, G. Zhu, B. Yu, A. Minnich, Y. Lan, X. Wang, M. Dresselhaus, Z. Ren, and G. Chen, Nano Lett. **11**, 2225 (2011).
[9]W. M. Steen, *Laser Material Processing* (Springer-Verlag, New York, 2010).
[10]J. F. Ready and D. F. Farson, *LIA Handbook of Laser Material Processing* (Magmplia, Orlando, 2001).
[11]D. Lin, C. R. Liu, and G. J. Cheng, J. Appl. Phys. **115**, 113513 (2014).
[12]Y. Gao, B. Wu, Y. Zhou, and S. Tao, Appl. Surf. Sci. **257**, 9960 (2011).
[13]E. V. Bordatchev, A. M. K. Hafiz, and O. R. Tutunea-Fatan, Int. J. Adv. Manuf. Tech. **73**, 35 (2014).
[14]A. M. K. Hafiz, E. V. Bordatchev, and R. O. Tutunea-Fatan, Int. J. Adv. Manuf. Tech. **70**, 1963 (2014).
[15]A. M. K. Hafiz, E. V. Bordatchev, and R. O. Tutunea-Fatan, J. Manuf. Processes **14**, 425 (2012).
[16]T. L. Perry, D. Werschmoeller, N. A. Duffie, X. Li, and F. E. Pfefferkorn, J. Manuf. Sci E.-T. ASME **131**, 021002 (2009).
[17]M. Vadali, C. Ma, N. A. Duffie, X. Li, and F. E. Pfefferkorn, J. Manuf. Processes **14**, 307 (2012).
[18]M. Vadali, C. Ma, N. A. Duffie, X. Li, and F. E. Pfefferkorn, J. Micro Nano Manuf. **1**, 011006 (2013).
[19]F. E. Pfefferkorn, N. A. Duffie, X. Li, M. Vadali, and C. Ma, CIRP Ann. Manuf. Technol. **62**, 203 (2013).
[20]C. Ma, M. Vadali, N. A. Duffie, F. E. Pfefferkorn, and X. Li, J. Manuf. Sci. E.-T. ASME **135**, 061023 (2013).
[21]C. Ma, M. Vadali, X. Li, N. A. Duffie, and F. E. Pfefferkorn, J. Micro Nano Manuf. **2**(2), 021010 (2014).
[22]D. B. Tuckerman and A. H. Weisberg, IEEE Electron Device Lett. **7**, 1 (1986).
[23]T. A. Mai and G. C. Lim, J. Laser Appl. **16**, 221 (2004).
[24]H. Wang, D. L. Bourell, and J. J. Beaman, in Proceedings of the 9th Solid Freeform Fabrication Symposium, Austin, US, 1998.
[25]M. Bereznai, I. Pelsöczi, Z. Tóth, K. Turzó, M. Radnai, Z. Bor, and A. Fazekas, Biomaterials **24**, 4197 (2003).
[26]Y. G. Kim, J. K. Ryu, D. J. Kim, H. J. Kim, S. Lee, B. H. Cha, H. Cha, and C. J. Kim, Jpn. J. Appl. Phys., Part 1 **43**, 1315 (2004).
[27]C. Nüsser, I. Wehrmann, and E. Willenborg, Phys. Procedia **12**, 462 (2011).
[28]F. E. Pfefferkorn, N. A. Duffie, J. D. Morrow, and Q. Wang, CIRP Ann. Manuf. Technol. **63**, 237 (2014).
[29]C. R. Heiple and J. R. Roper, Weld. J. **61**, 97-s (1982).
[30]Y. H. Ahmad and A. M. A. Mohamed, Int. J. Electrochem. Sci. **9**, 1942 (2014).
[31]B. Gallois and C. H. P. Lupis, Metall. Trans. B **12B**, 549 (1981).
[32]S. C. Chen, D. G. Cahill, and C. P. Grigoropoulos, ASME J. Heat Trans. Technol. **122**, 107 (2000).
[33]J. Lee, T. Tanaka, M. Yamamoto, and S. Hara, Mater. Trans. JIM **45**, 625 (2004).